PHILOSOPHICAL TRANSACTIONS OF THE ROYAL SOCIETY A MATHEMATICAL, PHYSICAL & ENGINEERING SCIENCES

Climate Studies with a Coupled Atmosphere--Upper-Ocean--Ice-Sheet Model

T. Fichefet, C. Tricot, A. Berger, H. Gallee and I. Marsiat

Phil. Trans. R. Soc. Lond. A 1989 **329**, 249-261
doi: 10.1098/rsta.1989.0074

Phil. Trans. R. Soc. Lond. A **329**, 249–261 (1989)
Printed in Great Britain

Climate studies with a coupled atmosphere–upper-ocean–ice-sheet model

By T. Fichefet, C. Tricot, A. Berger, H. Gallée and I. Marsiat
Institut d'Astronomie et de Géophysique G. Lemaître, Université Catholique de Louvain, B-1348 Louvain-la-Neuve, Belgium

A two-dimensional zonally averaged model has been developed for simulating the seasonal cycle of the climate of the Northern Hemisphere. The atmospheric component of the model is based on the two-level quasi-geostrophic potential vorticity system of equations. At the surface, the model has land–sea resolution and incorporates detailed snow and sea-ice mass budgets. The upper ocean is represented by an integral mixed-layer model that takes into account the meridional advection and turbulent diffusion of heat. Comparisons between the computed present-day climate and climatological data show that the model does reasonably well in simulating the seasonal cycle of the temperature field. In response to a projected CO_2 trend based on the scenario of Wuebbles *et al.* (*DOE/NBB*-0066 *Technical Report* 15 (1984)), the modelled annual hemispheric mean surface temperature increases by 2 °C between 1983 and 2063. In the high latitudes, the response undergoes significant seasonal variations. The largest surface warmings occur during autumn and spring. The model is then asynchronously coupled to a model that simulates the dynamics of the Greenland, the Eurasian and the North American ice sheets in order to investigate the transient response of the climate to the long-term insolation anomalies caused by orbital perturbations. Over the last interglacial–glacial cycle, the coupled model produces continental ice-volume changes that are in general agreement with the low-frequency part of palaeoclimatic records.

1. Introduction

The past two decades have seen an accelerated growth of interest in the Earth's climate and in its variations. This concern stems partly from the recognition that mankind is becoming a significant factor in the climatic balance of the Earth and partially from Man's increasing vulnerability to climatic fluctuations, whether they are natural or Man-induced. The urgency for climatic predictions has led to the development of numerous mathematical models of climate, ranging from simple zero-dimensional energy balance models (EBMs) to complex three-dimensional general circulation models (GCMs) (for general reviews, see Schneider & Dickinson 1974; Shine & Henderson-Sellers 1983; Meehl 1984).

Among this hierarchy of models, two-dimensional zonally averaged dynamical models have been, and will continue to be, a useful tool in climate research. This class of models has more sophisticated treatment of the atmospheric meridional processes than latitudinally dependent EBMs. Compared with GCMs, zonally averaged dynamical models have the peculiarities of the absence of synoptically generated climatic 'noise', thereby permitting the investigation of a range of climatic perturbations in which the forcing function is relatively small, and of greatly reduced computer requirements (MacCracken & Ghan 1988). This computational flexibility allows a large number of climate-sensitivity experiments to be done, helping to identify the role

and potential importance of specific physical processes for the present climate and for climatic changes. Results of these simulations can then be used as a guide to experiments that should be done with the more-sophisticated GCMs.

Results from such a zonally averaged dynamical model are presented in this work. The structure of the model is described in §2. The model simulation of the present-day climate of the Northern Hemisphere is then discussed in §3. Section 4 investigates the transient response of the model to future atmospheric carbon dioxide concentration. In §5, the model is coupled to an ice-sheet model to study the long-term transient response of the climate to the insolation variations caused by periodic changes in the Earth's orbital elements. Concluding remarks are given in §6.

2. Description of the model

Our model is a zonally averaged dynamical model specifically designed for simulating the seasonal cycle of the climate of the Northern Hemisphere. It has land–sea resolution at the surface level and takes into consideration the main physical interactions between the atmosphere, the upper ocean, the cryosphere (including sea ice, seasonal snow cover and ice sheets) and the surface lithosphere. A summary of the model characteristics is presented here; further details can be found in Gallée *et al.* (1989).

The atmospheric model is based on the zonally averaged form of the two-level quasi-geostrophic potential vorticity system of equations (including diabatic heating and frictional dissipation) written in spherical and pressure coordinates (Sela & Wiin-Nielsen 1971; Ohring & Adler 1978). The basic output consists of the latitudinal distribution of the temperature at 500 hPa and of the zonal winds at 250 hPa and 750 hPa. Meridional transport of quasi-geostrophic potential vorticity is accomplished by an eddy-mixing process with exchange coefficients parametrized as in Gallée (1987). The quasi-geostrophic approximation leads to an underestimation of the strength of the Hadley cell in the low latitudes and, therefore, to an overestimation of the temperatures in these regions. To partly remedy this problem, a parametrization of the vertically integrated Hadley heat transport (Peng *et al.* 1987) has been introduced in the model. Separate surface-energy balances are calculated over various surface types at each latitude and the heating of the atmosphere because of the vertical heat fluxes is the weighted average of the convergences of these fluxes above each kind of surface. The vertical heating processes considered are solar radiation, longwave radiation, convection and latent heat release.

The solar radiation scheme used here is very similar to the one described by Tricot & Berger (1988). The following processes are included: absorption by water vapour, carbon dioxide and ozone, Rayleigh scattering, absorption and scattering by cloud droplets and aerosols, and reflection by the surface. The longwave-radiation computations are based on Morcrette's (1984) wide-band formulation of the radiative transfer equation for use in GCMs. Absorption by water vapour, carbon dioxide and ozone is explicitly treated and the cloud cover is supposed to behave as a blackbody, as is the surface of the Earth. In both schemes, account is taken of variation in surface topography.

The calculation of the radiative fluxes requires a knowledge of the vertical temperature profile and of the vertical distribution of the main optically active atmospheric constituents above the different surface types. Given the model-predicted zonally averaged temperature at 500 hPa, the vertical temperature profile in the troposphere is determined by assuming that the

PHILOSOPHICAL TRANSACTIONS OF THE ROYAL SOCIETY A MATHEMATICAL, PHYSICAL & ENGINEERING SCIENCES

product of the static stability parameter by the pressure is constant throughout that layer (Wiin-Nielsen & Sela 1971). Near the surface, this temperature profile is gradually modified so that the surface air temperature is equal to the surface temperature. The stratosphere is supposed to be isothermal with a temperature identical to that of the tropopause. Tropopause height is parametrized as a function of the zonally averaged surface temperature after Sellers (1983). The vertical variation of specific humidity is deduced from the surface temperature and relative humidity according to Smith (1966). Mean annual climatological values of relative humidity are used separately over continental and oceanic surfaces. The carbon dioxide concentration is taken to be constant in space and time. The ozone mixing ratio is specified as a function of latitude, height and time from observations. Three kinds of aerosols are considered: continental, maritime and unperturbed stratospheric. An effective single cloud is assumed to exist in each latitude belt, with monthly cloud amount prescribed from climatology. The base and top altitudes of the cloud layer are kept fixed throughout the year. Finally, the value of the solar constant is taken to equal 1368 W m^{-2}.

The transfer of sensible heat from the surface to the atmosphere by convection is parametrized according to Saltzman & Ashe (1976). The latent heat release in the atmosphere is obtained from observed zonal and monthly mean precipitation rates uniformly scaled to ensure a balance between precipitation and surface evaporation (computed as in Saltzman 1980) over the whole hemisphere.

At each latitude, the model surface is basically resolved into continental and oceanic portions. Land can be partly covered by snow and by a maximum of three ice sheets representing the Greenland, the Eurasian and the North American ice sheets. For the present climate, the fraction of the land area occupied by the two latter ice sheets is zero at all latitudes and the altitude and extent of the Greenland ice sheet are specified from data. The zonally averaged elevation of the ice-free land is deduced from present-day observations. Sea ice can exist at the ocean surface and vary in amount at the expense of the open water area.

Over the land free of snow and ice, the surface temperature is determined by applying the force restore method of Bhumralkar (1975) and Blackadar (1976). The ground water budget is calculated by the so-called bucket method (Manabe *et al.* 1981). The soil is assumed to have a water-holding capacity of 40 cm. If the calculated soil moisture exceeds this value, the excess is supposed to run off. Changes in soil moisture are computed from the rates of rainfall, evaporation, snow melt, and run-off.

The fraction of the land area above which precipitation falls as snow is parametrized as a function of the surface temperature following Harvey (1988). The surface temperature of the snow layer is obtained by assuming a thermal equilibrium between the internal conductive heat flux and the other surface heat fluxes. When the predicted temperature reaches 0 °C, snow melt occurs. The melting is partitioned between a decrease in snow extent and a decrease in snow depth, so that snow area is gradually reduced during the snow melt period.

Over the ice sheets, the proportion of precipitation falling as snow depends on the surface temperature as in Ledley (1985). The temperature at the air–snow interface is deduced from an energy-balance equation similar to the one used for snow on land. An explicit surface mass budget provides the net accumulation rate of snow.

The upper ocean is represented by the variable depth and temperature mixed-layer model of Gaspar (1988). To simulate the oceanic heat transport and its influence upon the sea surface temperature, a parametrization of the meridional advection of heat by wind-driven oceanic

PHILOSOPHICAL TRANSACTIONS OF THE ROYAL SOCIETY A MATHEMATICAL, PHYSICAL & ENGINEERING SCIENCES

currents (Sellers 1976) and of the horizontal turbulent diffusion of heat (Sellers 1973) has been included in the model. No exchange of heat is allowed between the mixed layer and the deeper ocean layers.

When the mixed-layer temperature falls below −2 °C, sea ice forms and covers a portion of the ocean area. In the presence of sea ice, the mixed-layer depth is kept fixed at 30 m because processes related to salinity that govern the mixed-layer dynamics in the polar regions (see, for example, Fichefet & Gaspar 1988) are not treated in this study. The surface temperature of the ice pack and the vertical ice growth or decay rates are calculated by using the zero-layer model of Semtner (1976). Snow on the top of the ice layer is not accounted for and no dynamic effects, such as ice drifting caused by wind, are considered. The opening and closing of leads and the open-water temperature are computed following the technique of Parkinson & Washington (1979). The heat flux from the ocean to the ice is calculated by assuming that sea ice is in thermodynamic equilibrium with the water just below. Therefore, both the temperature at the base of the ice and the temperature of the water under the ice are supposed to be equal to −2 °C. In the model, the only physical mechanism that can disturb this equilibrium is a partial mixing between the water under the ice and the water in the leads. To maintain the water at −2 °C, the heat flux from the ocean to the ice has to compensate exactly for that perturbation.

Albedos are different over land, snow, ocean, and sea ice. The albedo of land not covered by snow or ice is a function of the soil liquid-water content according to Saltzman & Ashe (1976). Over the continental surfaces located northward of the annual mean −5 °C isotherm and over ice sheets, the snow albedo is dependent on the surface temperature and the snow age as in Danard *et al.* (1984). The maximum albedo of snow is assumed to be 0.85 for fresh snowfall on a frozen snow pack and 0.70 for fresh snowfall on melting snow cover. Everywhere else, the snow albedo is fixed at a constant value of 0.4 (Robock 1980). The albedo of ice-free ocean under clear sky is parametrized as a function of solar zenith angle after Briegleb & Ramanathan (1982). Under cloudy conditions the albedo of the ocean is set to be 0.07. The albedo of sea ice is assumed to vary linearly with temperature, from 0.75 at −10 °C to 0.40 at 0 °C (Robock 1980).

In all the experiments presented below, a latitudinal resolution of 5° and a time step of 3 days were used.

3. Simulation of present climate

The model described in §2 was first used to simulate the present climate of the Northern Hemisphere. This experiment was performed by assuming a CO_2 concentration of 330 parts per million by volume (p.p.m.v.). Starting from arbitrary initial conditions, the model was run until an equilibrium seasonal cycle was established. This equilibrium was achieved when the annual hemispheric mean radiative balance at the top of the atmosphere became less than 0.1 W m^{-2}. This was reached after 20 years of integration.

The seasonal cycle of the temperature at 500 hPa simulated by the model is depicted in figure 1*a*. The magnitude and horizontal gradient of the temperature are generally in good quantitative agreement with the monthly mean data of Oort (1983). A plot of the difference between the predicted and observed temperatures in figure 1*b* shows that the major discrepancy occurs during winter in the tropics where the modelled temperature is underestimated by 4 °C. This error relates partly to the way the atmospheric model calculates the meridional heat transport in these regions. In middle and high latitudes, the computed

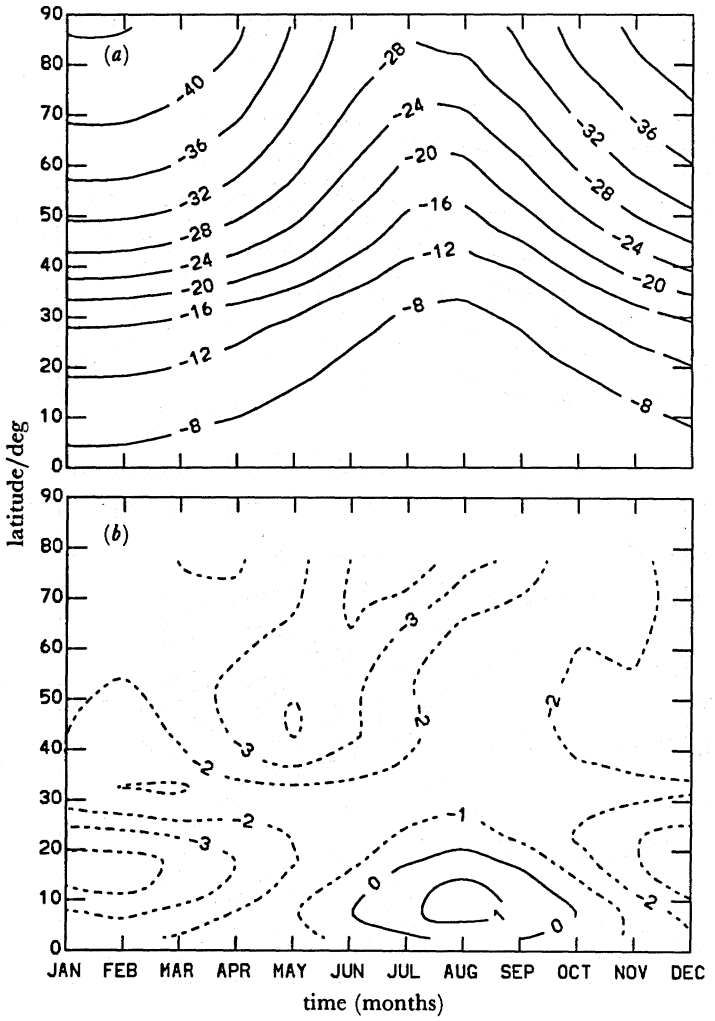

FIGURE 1. Latitude–time distribution of the zonal mean temperature at 500 hPa simulated by the model (*a*) and of the difference between the computed temperature and the observations of Oort (1983) (*b*). The units are degrees Celsius. Broken line denotes negative deviation.

temperature is about 3 °C too cold during spring. This is mostly caused by an overestimation of the snow extent at the beginning of the melting period.

Figure 2*a* illustrates the seasonal cycle of the mixed-layer temperature predicted by the model. The departure of the simulated temperature from the observed one (Levitus 1982) is displayed in figure 2*b*. This figure shows temperature differences less than 2 °C almost everywhere. However, near 50° N, the mixed layer is 4–5 °C too warm during summer months. This behaviour is mainly a result of an insufficient vertical mixing of the spring and summer surface heat input, which is caused by an underestimation of the surface wind speed. At the same time, the mixed layer temperature is 4 °C too low near 70° N. The causes of this discrepancy have not yet been completely identified. It may arise in part from the use of a zonally averaged ocean model.

Further evidence of the model performance for present-day climate is given in Gallée *et al.* (1989). This paper demonstrates that the model shows acceptably good agreement with enough aspects of the behaviour of the real climate system to permit useful study of a range of possible environmental perturbations.

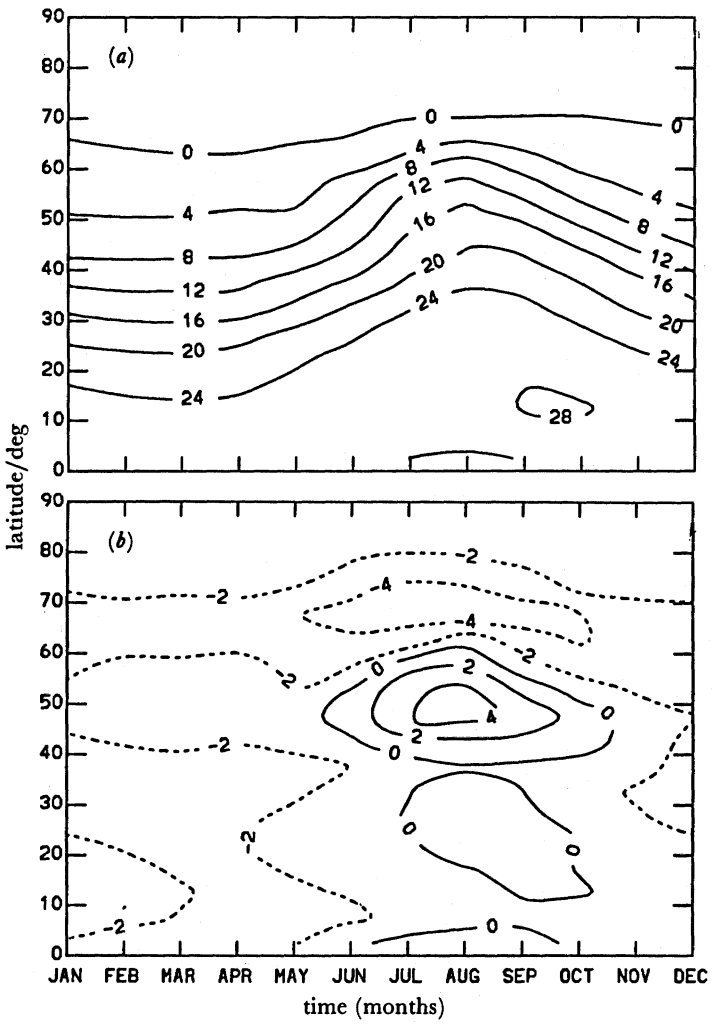

FIGURE 2. Latitude–time distribution of the zonal mean sea surface temperature simulated by the model (*a*) and of the difference between the computed temperature and the observations of Levitus (1982) (*b*). The units are degrees Celsius. Broken line denotes negative deviation.

4. TRANSIENT RESPONSE OF CLIMATE TO PROJECTED CO_2 INCREASE

In recent years the focus of studying the effect of increasing atmospheric CO_2 and other greenhouse gases has shifted from equilibrium climate response to transient response (see, for example, Wigley & Schlesinger 1985; Tricot & Berger 1987). The time-dependent response of climate to an increase in greenhouse-gas concentrations is likely to be slowed by the large thermal inertia of the ocean. Moreover, because the effective thermal inertia of the ocean is dependent on the ocean circulation and varies with latitude, it is possible that the transient response of the climate to enhanced greenhouse-gas concentrations could differ substantially from the equilibrium response (Schneider & Thompson 1981).

The transient response of our model to a projected CO_2 concentration increase in the near future is investigated here. The model was first run to reach equilibrium with a CO_2 concentration of 341 p.p.m.v., corresponding to the year 1983 (the control run). The model run was then continued up to 2063 with the CO_2 concentration changing in time according

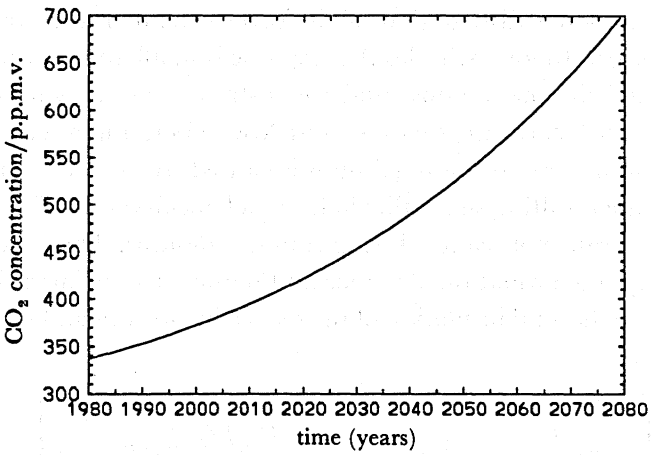

FIGURE 3. Time-dependent scenario for future atmospheric CO_2 concentration (after Wuebbles *et al.* 1984).

to the scenario plotted in figure 3. This selected scenario predicts a CO_2 concentration of 600 p.p.m.v. in 2063.

Figure 4 shows the transient response of the annual and zonal mean surface temperature given by the difference between the actual transient climatic state and the control run. The figure indicates a continuous warming over the whole hemisphere that is particularly pronounced in high latitudes. The surface warming between 1983 and 2063 reaches nearly 6 °C around 80° N and 4 °C around 70° N. In middle latitudes, the surface temperature increase is about 2 °C and in lower latitudes the warming ranges between 1 °C and 1.5 °C. The annual hemispheric mean surface warming is 2 °C.

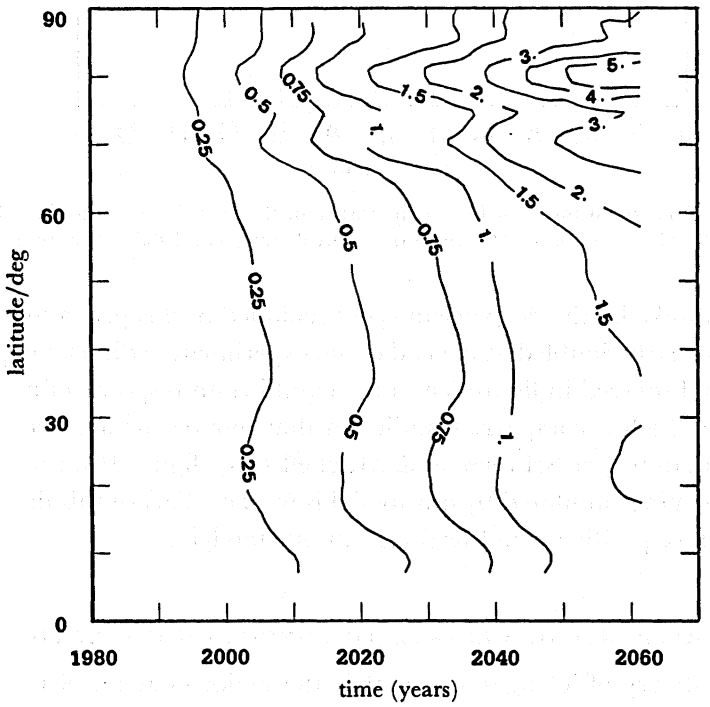

FIGURE 4. Transient response of the annual and zonal mean surface temperature to the time-dependent CO_2 increase shown in figure 3. The response is relative to the control run (year 1983). The units are degrees Celsius.

The latitudinal and seasonal distribution of the surface temperature response in the year 2063 is presented in figure 5. In low latitudes the response is small and very uniform with season and latitude. In high latitudes the response undergoes strong seasonal variations, with a major maximum of 12 °C at *ca.* 80° N during October and November, and a secondary maximum of 7 °C at *ca.* 70° N in March. The spring maximum is caused by an earlier melting of the snow cover over land and to the resulting snow albedo feedback mechanism. The autumn maximum is caused by the disappearance of sea ice during summer months. The excess of heat received by the mixed layer delays the formation of sea ice and reduces its thickness during winter. This leads to a reduction of the thermal insulation of the sea ice in autumn and early winter (Fichefet 1988*a*).

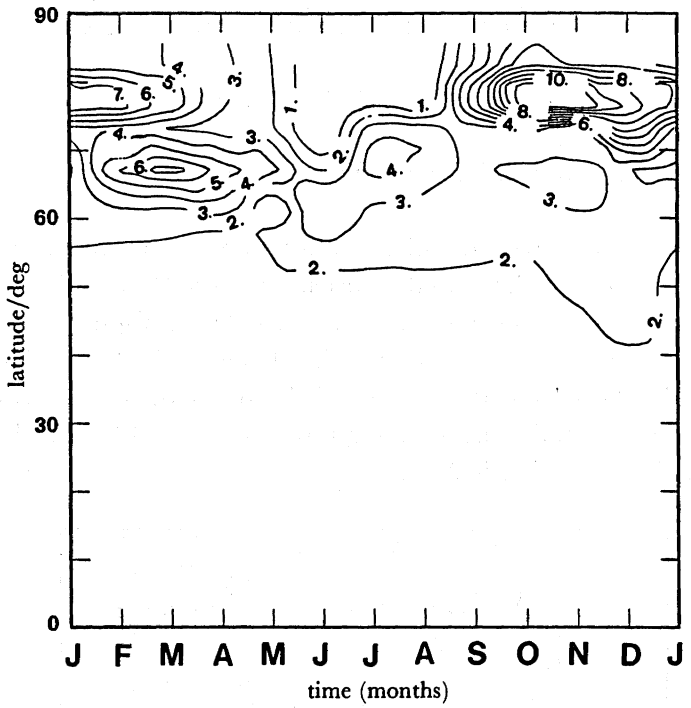

FIGURE 5. Response of the zonal mean surface temperature in the year 2063 to the time-dependent CO_2 increase shown in figure 3. The response is relative to the control run (year 1983). The units are degrees Celsius.

Because the heat uptake by the deep ocean is not included in this preliminary study and the CO_2 concentration is nearly doubled at the end of the experiment, a direct comparison between temperature changes displayed in figure 5 and the equilibrium response of GCMs to a doubling of CO_2 can be made. Such a comparison indicates that our results are very similar to those obtained recently with GCMs (see Schlesinger & Mitchell 1987, figure 16), except in the tropical regions where the warming simulated by our model is weaker. Part of this discrepancy may be explained by the lack of positive cloud feedback in our model.

5. TRANSIENT RESPONSE OF CLIMATE TO LONG-TERM INSOLATION CHANGES

The astronomical theory of ice ages asserts that the major changes of the Earth's climate during late Quaternary are the consequence of the seasonal and latitudinal redistribution of the extraterrestrial insolation resulting from pertubations of the orbital elements of the Earth

(Milankovitch 1941; Berger *et al.* 1984). This theory has received substantial support from detailed analysis of deep-sea sedimentary cores (see Hays *et al.* 1976), but the question as to what processes in the climate system are responsible for the translation of the relatively modest changes in insolation into large variations in continental ice volume remains unsettled.

Simple axisymmetric ice-sheet models have been used in the past to predict the time evolution of ice thickness as a function of latitude. The inclusion of isostatic land movements in these models tends to improve their ability to reproduce global climate features that are recorded in late-Quaternary deep-sea core records. However, such models have usually used a prescribed snow mass-budget distribution whose sensitivity to insolation perturbations was specified rather arbitrarily (see Hyde & Peltier 1987).

To analyse the transient response of the climate to the long-term insolation anomalies, the seasonal climate model presented in §2 has been coupled to a model that simulates the zonally averaged dynamics of the Greenland, the Eurasian and the North American ice sheets. The evolution of the ice thickness is computed along a meridian by using the conservation equation of ice mass (Oerlemans 1980). A lateral ice flow is operating at each latitude with the assumption that the east–west profile of the ice sheets is parabolic. Contrary to the majority of previous studies, the annual mean accumulation rates of snow at the ice surface are explicitly calculated by the seasonal climate model as the local excess or deficit of snowfall over snow melt. The long-term response of the underlying bedrock to the ice load is computed according to the formulation of Oerlemans & Van der Veen (1984). Latitudinal grid spacing is 0.5° and the time step is one year.

The most efficient way to undertake the coupling between the seasonal-climate model and the ice-sheet model is to run the two models asynchronously. Therefore, a long-term experiment will consist of a repetition of loops, each loop composed of two parts, one associated with the relatively fast response of the seasonal-climate model and one with the slower response of the ice-sheet model. In the first part, the orbital parameters are calculated for a particular geological time by applying the equations of Berger (1978). The seasonal-insolation cycle associated with these parameters is then determined. By using this solar forcing and assuming that the elevation of the ice sheets is known, the seasonal-climate model is integrated until an equilibrium seasonal cycle is approached. For the second part of the loop, the equilibrium solution is used to find annual mean accumulation rates of snow over the ice sheets. Holding these constant and by using the previous elevation of the ice sheets as initial conditions, the ice sheet model is run for 2000 years. With the new topography of the ice sheets as surface boundary condition and with the updated orbital parameters, the loop is repeated.

Such a coupling technique was undertaken to simulate the low-frequency part of the evolution of the climate system over the last interglacial–glacial cycle. This geological period extends from around 125000 years before present (125 ka BP) to present time and was chosen because it is well dated and amply documented. For that long-term experiment, the infrared calculations were highly simplified to reduce computer expense (Berger *et al.* 1988) and the CO_2 concentration was kept fixed at 330 p.p.m.v. The simulation was started at 122 ka BP assuming that there was no continental ice in the Northern Hemisphere, except over Greenland. Although the size of the Greenland ice sheet during the last interglacial period is not known precisely, its surface elevation was probably lower than today (Dansgaard *et al.* 1982). Therefore, it was supposed that the Greenland ice sheet volume was two thirds of its present value at the beginning of the simulation. All along the run, which was carried out using

PHILOSOPHICAL TRANSACTIONS OF THE ROYAL SOCIETY A MATHEMATICAL, PHYSICAL & ENGINEERING SCIENCES

the coupling scheme described above, new ice sheet was initiated in a latitudinal belt whenever the annual snow mass budget was positive in the seasonal-climate model.

Figure 6 shows the simulated variation of the total continental ice volume as a function of time compared with the sea-level curve of Chappell & Shackleton (1986). This ice volume includes the contribution of Antarctica, based on the reconstruction of Hughes *et al.* (1981).

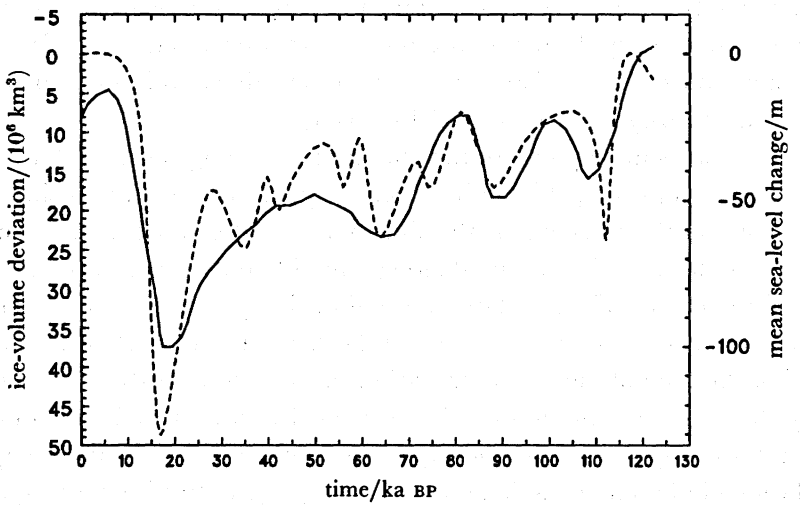

FIGURE 6. Variations over the last interglacial–glacial cycle of (i) the deviation of the total continental ice volume over the Earth from present-day value simulated by the coupled model (full line, left scale), and (ii) the mean sea-level change given by Chappell & Shackleton (1986) (broken line, right scale).

The main characteristic of this figure is the general agreement between the reconstructed and the modelled ice volume on the 10 ka timescale. However, the present simulation seems to underestimate the maximum ice volume around 18 ka BP. This feature may be partly explained by the fact that the model does not include sea-level changes, and thus does not allow the ice sheets to extend over the continental shelves. On the other hand, the model overestimates the total ice volume between 10 ka BP and present. This discrepancy is probably because of the neglect, in the present work, of additional physical processes that can affect the surface energy balance (e.g. variations in atmospheric CO_2 content) or that can change the ice dynamics (e.g. the ice flow–temperature interaction).

The simulated time evolution of the three ice sheets and the total ice volume in the Northern Hemisphere is illustrated in figure 7. At 120 ka BP, the early summer insolation conditions are such that the continents begin to accumulate perennial snow at latitudes greater than 75 °N. So the Greenland ice sheet exhibits growth and the North American ice sheet begins to form, the Eurasian ice sheet is initiated 2 ka later. The rapid and strong variations of the insolation pattern prevent the size of the ice sheets from increasing very much before 70 ka BP. Although the summer insolation deficit is not very significant around 70 ka BP, the existence of the ice sheets at 80 ka BP together with the absence of an important summer solar excess after 70 ka BP allows a large growth of the ice volume everywhere. Afterwards, the simulation shows first a slow decrease in ice volume between 64 ka BP and 50 ka BP followed by a slow ice volume increase up to 30 ka BP and a faster subsequent increase up to the last glacial period around 18 ka BP. The Greenland ice sheet reaches its largest size at 22 ka BP and those of Eurasia and

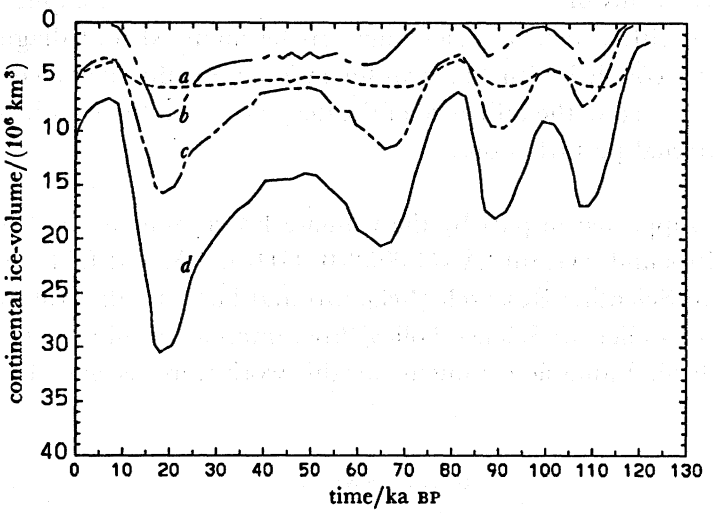

FIGURE 7. Variations over the last interglacial–glacial cycle of the ice volume simulated by the coupled model over Greenland (curve *a*), Eurasia (curve *b*), North America (curve *c*) and the whole Northern Hemisphere (curve *d*).

North America 4 ka later. This difference is a result of the impossibility of the Greenland ice sheet extending southward of 60° N. When the ice sheets become large, their increasing altitudes limit the potential amount of snowfall in the model following a simple parametrization. This feature affects both snow accumulation and albedo, which decreases with time when snowfall diminishes. Therefore, when early summer insolation increases after 24 ka BP, the relatively low albedo of the ice sheets effectively increases the amount of solar energy input to the system, which in turn restores a positive energy balance at the ice-sheet surface. This leads to a surface-temperature increase and melting is favoured, causing an additional albedo decrease. Ablation at the southern tip of the ice sheets becomes so important that a depression in the ice forms there. Ice then flows rapidly into this depression. The altitude of the ice sheets decreases everywhere and the ablation zone becomes predominant. Rapid deglaciation up to 6 ka BP is thus a consequence of these feedback mechanisms, which are initiated by a slight increase in insolation at a time where the maximum volume of ice makes the ice sheets more vulnerable. The Eurasian ice sheet totally disappears at 6 ka BP. The remaining ice volumes over Greenland and North America are overestimated at that time. After 6 ka BP, the decrease in summer insolation and the existence of the high surface albedos allow these ice sheets to start growing again, contrary to observation.

6. CONCLUSIONS

A two-dimensional zonally averaged dynamical model has been developed for use in climate sensitivity studies. The model has demonstrated its ability to simulate the present-day climate of the Northern Hemisphere. A preliminary experiment has proven its potential usefulness for studying problems involving the transient response of climate to the increase in greenhouse-gas concentrations. Moreover, when the dynamics of the ice sheets is taken into consideration, the model is able to reproduce global ice-volume changes over the last interglacial–glacial cycle that are in general agreement with the low-frequency part of recent geological reconstructions.

PHILOSOPHICAL TRANSACTIONS OF THE ROYAL SOCIETY A MATHEMATICAL, PHYSICAL & ENGINEERING SCIENCES

The main advantages of this physically-based climate model are its computational efficiency and the relative ease with which its behaviour can be analysed and diagnosed. In future experiments, it will be coupled with the two-dimensional zonally averaged ocean model of Fichefet (1988*b*) to investigate the influence of the deep ocean on the transient response of the climate system to external perturbations.

This research was supported in part by the Climate Programme of the Commission of the European Communities under Grant EV4C-0052-B (GDF). T.F. and I.M. were sponsored by the National Fund for Scientific Research (Belgium) and H.G. by the Antarctic Programme of the Prime Minister's Office for Science Policy Programming (Belgium). These supports are gratefully acknowledged. Valuable comments on this work were received from H. Cattle.

References

Berger, A. 1978 *J. atmos. Sci.* **35**, 2363–2367.
Berger, A., Gallée, H., Fichefet, T., Marsiat, I. & Tricot, C. 1988 *Scientific report* 1988/3 Institut d'Astronomie et de Géophysique G. Lemaître, Université Catholique de Louvain.
Berger, A., Imbrie, J., Hays, J., Kukla, G. & Saltzman, B. (ed.) 1984 *Milankovitch and climate*. Dordrecht: D. Reidel Publishing Company.
Blackadar, A. K. 1976 In *Proceedings of the third symposium on atmospheric turbulence, diffusion and air quality*, pp. 46–49. Boston: American Meteorological Society.
Bhumralkar, C. M. 1975 *J. appl. Met.* **14**, 1246–1258.
Briegleb, B. & Ramanathan, V. 1982 *J. appl. Met.* **21**, 1160–1171.
Chappell, J. & Shackleton, N. J. 1986 *Nature, Lond.* **324**, 137–140.
Danard, M., Gray, M. & Lyv, G. 1984 *Mon. Wea. Rev.* **112**, 1160–1169.
Dansgaard, W., Clausen, H. B., Gundestrup, N., Hammer, C. U., Johnsen, S. F., Kristindottir, P. M. & Reeh, N. 1982 *Science, Wash.* **218**, 1273–1277.
Fichefet, T. 1988*a* Thesis, Université Catholique de Louvain.
Fichefet, T. 1988*b* Ph.D. thesis, Université Catholique de Louvain.
Fichefet, T. & Gaspar, P. 1988 *J. phys. Oceanogr.* **18**, 181–195.
Gallée, H. 1987 *Progress report* 1987/4 Institut d'Astronomie et de Géophysique G. Lemaître, Université Catholique de Louvain.
Gallée, H., van Ypersele, J. P., Fichefet, T., Marsiat, I., Tricot, C. & Berger, A. 1989 *Scientific report* 1989/3 Institut d'Astronomie et de Géophysique G. Lemaître, Université Catholique de Louvain.
Gaspar, P. 1988 *J. phys. Oceanogr.* **18**, 161–180.
Harvey, L. D. D. 1988 *J. Climate* **1**, 1065–1085.
Hays, J. D., Imbrie, J. & Shackleton, N. 1976 *Science, Wash.* **194**, 1121–1132.
Hughes, T. J., Denton, G. H., Anderson, B. G., Schilling, D. H., Fasthook, J. L. & Lingle, C. S. 1981 In *The last great ice sheets* (ed. G. H. Denton & T. J. Hughes), pp. 275–317. New York: John Wiley & Sons.
Hyde, W. T. & Peltier, W. R. 1987 *J. atmos. Sci.* **44**, 1351–1374.
Ledley, T. S. 1985 *J. geophys. Res.* **90**, 2251–2260.
Levitus, S. 1982 *Climatological atlas of the world ocean, NOAA professional paper no.* 13. Washington, D.C.: U.S. Government Printing Office.
MacCracken, M. C. & Ghan, S. J. 1988 In *Physically-based modelling and simulation of climate and climatic change – Part II* (ed. M. E. Schlesinger), pp. 755–809. Dordrecht: Kluwer Academic Publishers.
Manabe, S., Wetherald, R. D. & Stouffer, R. J. 1981 *Climatic Change* **3**, 347–386.
Meehl, G. A. 1984 *Climatic Change* **6**, 259–286.
Milankovitch, M. 1941 *Canon of insolation and the ice age problem. K. Serb. Acad. Beogr. Spec. Pub.* 132 (English translation by Israel Program for Scientific Translation and published for the U.S. Department of Commerce and the National Science Foundation).
Morcrette, J. J. 1984 Ph.D. thesis, Université des Sciences et Techniques de Lille.
Oerlemans, J. 1980 *Nature, Lond.* **287**, 430–432.
Oerlemans, J. & Van der Veen, C. J. 1984 *Ice sheets and climate*. Dordrecht: D. Reidel Publishing Company.
Ohring, G. & Adler, S. 1978 *J. atmos. Sci.* **35**, 186–205.
Oort, A. H. 1983 *Global atmospheric circulation statistics, 1958–1973, NOAA professional paper no.* 14. Washington, D.C.: U.S. Government Printing Office.
Parkinson, C. L. & Washington, W. M. 1979 *J. geophys. Res.* **84**, 311–337.

PHILOSOPHICAL TRANSACTIONS OF THE ROYAL SOCIETY A MATHEMATICAL, PHYSICAL & ENGINEERING SCIENCES

Peng, L., Chou, M. D. & Arking, A. 1987 *J. geophys. Res.* **92**, 5505–5521.
Robock, A. 1980 *Mon. Wea. Rev.* **108**, 267–285.
Saltzman, B. 1980 *Arch. Met. geophys. Biokl.* **29**A, 41–53.
Saltzman, B. & Ashe, S. 1976 *Tellus* **28**, 307–322.
Schlesinger, M. E. & Mitchell, J. F. B. 1987 *Rev. Geophys.* **25**, 760–798.
Schneider, S. H. & Dickinson, R. E. 1974 *Rev. Geophys. space Phys.* **12**, 447–493.
Schneider, S. H. & Thompson, S. L. 1981 *J. geophys. Res.* **86**, 3135–3147.
Sela, J. & Wiin-Nielsen, A. 1971 *Mon. Wea. Rev.* **99**, 460–468.
Sellers, W. D. 1973 *J. appl. Met.* **12**, 241–253.
Sellers, W. D. 1976 *Mon. Wea. Rev.* **104**, 233–248.
Sellers, W. D. 1983 *J. Clim. appl. Met.* **22**, 1557–1574.
Semtner, A. J. 1976 *J. phys. Oceanogr.* **6**, 379–389.
Shine, K. P. & Henderson-Sellers, A. 1983 *J. Climatol.* **3**, 81–94.
Smith, W. L. 1966 *J. appl. Met.* **5**, 726–727.
Tricot, C. & Berger, A. 1987 *Climate Dynam.* **2**, 39–61.
Tricot, C. & Berger, A. 1988 In *Long and short term variability of climate* (ed. H. Wanner & U. Siegenthaler), pp. 132–152. Berlin: Springer-Verlag.
Wigley, T. M. L. & Schlesinger, M. E. 1985 *Nature, Lond.* **315**, 649–652.
Wiin-Nielsen, A. & Sela, J. 1971 *Mon. Wea. Rev.* **99**, 447–459.
Wuebbles, D. J., MacCracken, M. C. & Luther, F. M. 1984 *DOE/NBB-0066 Technical Report* 15.

PHILOSOPHICAL TRANSACTIONS OF THE ROYAL SOCIETY A MATHEMATICAL, PHYSICAL & ENGINEERING SCIENCES